Available online at www.sciencedirect.com

SciVerse ScienceDirect

Ceramics International 38 (2012) 5723–5730

CERAMICS INTERNATIONAL

www.elsevier.com/locate/ceramint

C/C–ZrC composite prepared by chemical vapor infiltration combined with alloyed reactive melt infiltration

Yonggang Tong *, Shuxin Bai, Ke Chen

College of Aerospace and Materials Engineering, National University of Defense Technology, Changsha 410073, PR China

Received 31 January 2012; received in revised form 29 March 2012; accepted 5 April 2012
Available online 13 April 2012

Abstract

A high performance and low cost C/C–ZrC composite was prepared by chemical vapor infiltration combined with zirconium–silicon (Zr: 91.2 at.%; Si: 8.8 at.%) alloyed reactive melt infiltration. The density of the as-received composite is 2.46 g/cm^3 and the open porosity is 5%. Due to the reaction between the pyrolytic carbon and Zr–Si alloy in the composite, ZrC and Zr_2Si phases were formed, the formation and distribution of which were investigated by thermodynamics and phase diagram. The as-received C/C–ZrC composite, with the flexural strength of 239.5 MPa, displayed a pseudo-ductile fracture behavior. Ablation properties of the C/C–ZrC composite were tested by a pulse laser. The linear ablation rate was 0.028 mm/s. A ZrO_2 barrier layer was formed on the ablation surface and the composite presented excellent ablation resistance.

Keywords: B. Microstructure; C. Mechanical properties; Reactive melt infiltration; C/C–ZrC composite

1. Introduction

Ultra high temperature materials (UHTMs) capable of prolonged operation in oxidizing environments at temperatures above 2000 °C are required for future space systems such as advanced hypersonic vehicles and rocket propulsion systems. The most widely studied UHTMs are refractory carbide/boride ceramics and C/C composite. C/C composite has many excellent properties such as low density, high specific strength, high thermal conductivity, and high resistance to thermal shock [1]. Nevertheless, C/C composite begins to oxidize over 400 °C and cannot meet the requirements any more because of their rapid ablation at ultrahigh temperature [2]. It is necessary to improve its ablation resistance at ultrahigh temperatures in oxidizing atmosphere. Refractory carbide/boride ceramics, known as ultra high temperature ceramics (UHTCs), can withstand the extreme thermal and chemical environments due to their high melting temperatures, high hardness, excellent oxidation and ablation resistance at high temperatures [3,4]. However, like most other kinds of ceramics, refractory carbide/boride ceramics are brittle and have a tendency toward catastrophic failure, for which their applications are limited.

If the high oxidation and ablation resistance of refractory carbide/boride ceramics and the excellent mechanical properties of C/C composite can be combined, C/C–UHTC composites of even higher performances may be obtained. In the last few years, many efforts have been made to develop the C/C–UHTC composites by introducing refractory carbide/boride compounds into C/C matrix. ZrB_2, HfC, TaC, SiC and ZrC were respectively introduced into C/C composite to improve the ablation resistance by slurry infiltration, liquid precursor route or chemical vapor infiltration [5–9], by which the ablation resistance of the C/C composite was improved. However, because the introduced refractory carbide/boride content is low, the reduction effect in the erosion of the C/C composite is limited.

Reactive melt infiltration (RMI) has been demonstrated to be an effective fabrication route for ceramic matrix composite (CMC). The ceramic matrix is obtained by the reaction between the porous preform and infiltrated metal melt. The driving force for infiltration is capillarity and the process finishes within minutes to hours. The RMI possess has many advantages including short fabrication period, low cost, and near net shape

* Corresponding author. Tel.: +86 731 4576147; fax: +86 731 4574791.
E-mail address: tygiaarh419@163.com (Y. Tong).

0272-8842/$36.00
http://dx.doi.org/10.1016/j.ceramint.2012.04.017

[10,11]. It is an effective method to introduce refractory carbide/boride compounds into C/C matrix. C/C–ZrC composite has been successfully fabricated by infiltrating C/C preform with zirconium melt [12,13]. Great mount of ZrC were introduced into C/C composite by the reaction between carbon and infiltrated zirconium, and the oxidation and ablation resistance of C/C composite was greatly improved. However, the C/C–ZrC composite was fabricated at a temperature higher than the melting point of zirconium (1855 °C), at which the carbon fibre properties tend to degrade. In this paper, C/C–ZrC composite was fabricated by alloyed reactive melt Infiltration. The eutectic zirconium–silicon alloy (Zr: 91.2 at.%; Si: 8.8 at.%) with the melting point of only 1570 °C was chosen to infiltrate the C/C preform. Because of the 8.8 at.% silicon added in the molten melt, the infiltration could be operated at a much lower temperature and multiple matrix composed of zirconium, carbon and silicon was obtained.

2. Experimental

2.1. Materials preparation

2.1.1. Preparation of porous C/C preforms

Carbon fibre needled felts were used as preform. The carbon fibre was polyacrylonitrile-based (T300, Toray, Japan). The needled felts were prepared by the three-dimensional needling technique, starting with repeatedly overlapping the layers of 0 non-woven fibre cloth, short-cut-fibre web, and 90 non-woven fibre cloth with needle-punching step by step. The pyrolytic carbon (PyC) was then deposited on the surface of the carbon fibres as the reaction carbon by chemical vapor infiltration process.

2.1.2. Preparation of C/C–ZrC composite

The porous C/C preforms were cut and polished with 3000-grit paper. It was ultrasonically cleaned with ethanol and dried at 150 °C for 4 h. The Zr–Si alloy (Zr: 91.2 at.%; Si: 8.8 at.%) was placed above the porous C/C preforms in a graphite pot, which was then placed in a high temperature furnace to prepare C/C–ZrC composite. The sample was heated to 1800 °C at a speed of 10 °C/min and the temperature was held for 10 min under the pressure of 8.0×10^{-2} Pa. Ar gas (99.99%) was then poured into the furnace to 1 atm and the furnace temperature was kept at 1800 °C for more than 20 min.

2.2. Properties test

The apparent density and open porosity were measured by Archimedes's method. Flexural strength was determined using a three-point-bending test on specimens of 50 mm × 4 mm × 3 mm with 40 mm span and 0.5 mm/min crosshead speed. The flexural strength was calculated from the values of three specimens under each test condition. Ablative resistance properties of the composite were tested by a pulsed laser. The laser power of 1000 W/cm^2 was selected to vertically irradiate on the materials exposed in the air.

2.3. Characterization

The morphology of the C/C–ZrC composite was observed by Hitachi-S4800 scanning electron microscope (SEM). The chemical composition was examined by energy dispersive spectroscopy (EDS). The phases of the sample were identified by X-ray diffraction (XRD, Rigaku D/Max 2550VB-) using Ni-filtered Cu Kα radiation at a scanning rate of 5°/min and scanning from 10° to 80° of 2θ.

3. Results and discussion

3.1. Density and open porosity of C/C preform and C/C–ZrC composite

Table 1 lists the bulk density and open porosity of the C/C preform and the obtained C/C–ZrC composite. The density of the composite increased from 1.33 g/cm^3 to 2.46 g/cm^3, while the open porosity decreased from 25.34% to 5.00% after melt infiltration. It is indicated that the Zr–Si melt was infiltrated into the C/C preform very well. The pores were filled and dense matrix was formed, which can also be confirmed by observing the microstructure of the C/C–ZrC composite (Fig. 1). As can be seen, the large pores among the fibre bundles have been sealed by the infiltrated melt, as well as some small apertures inside the fibre bundles.

ZrC was formed along PyC due to the in situ reaction between PyC and zirconium during the RMI process. The generated ZrC is dense and acts as a melt penetration barrier. As indicated by Adelsberg et al. [14], the growth rate of ZrC layer is quite high. Besides, reaction between C (molar volume $V_C = 5.3$ cm^3) and melting Zr with the formation of ZrC (molar volume $V_{ZrC} = 16$ cm^3) leads to a volume increase of 300%. Therefore, the reaction-formed ZrC is liable to retarding the next infiltration steps. That may be the reason why certain mount of pores still existed inside the reaction formed ZrC matrix in the work of Wang et al. [13]. However, the present work does not suffer from that problem. For the one hand, different from the normal pressure infiltration in argon atmosphere in the work of Wang et al. [13], vacuum infiltration combined with low pressure infiltration was applied to prepare the C/C–ZrC composite. The driving force for infiltration is capillarity, which owns an inverse relation with the pore's diameter [15]. The distribution of pores in the porous C/C preform is mainly in the range of 20–200 μm. The melt was more prone to infiltrate into the porous C/C preform with the help of vacuum and pressure before the small pores were retarded. For the other, because the melting point of the Zr–Si alloy used in present work (1570 °C), in which the concentration of silicon is 8.8 at.%, is 275 °C lower than that of pure zirconium,

Table 1
Density and open porosity of the C/C preform and the as-received C/C–ZrC composite.

	C/C preform	C/C–ZrC composite
Density (g/cm^3)	1.33	2.46
Open porosity (%)	25.34	5.00

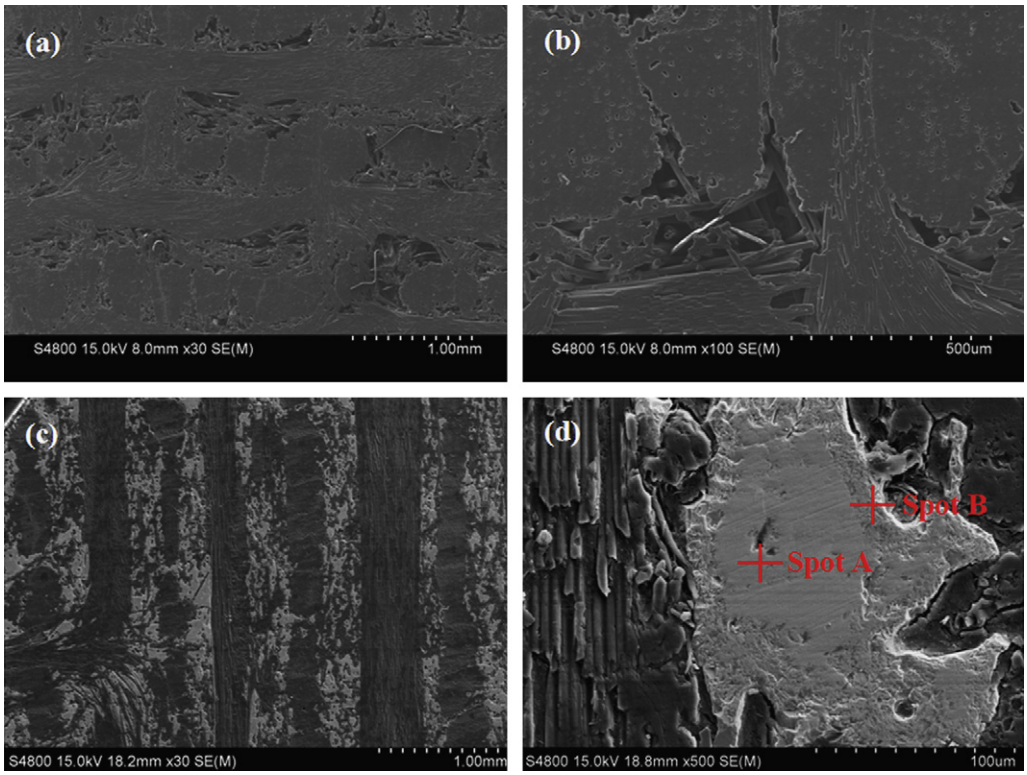

Fig. 1. Microstructure of the C/C preform and the as-received C/C–ZrC composite: (a and b) C/C preform and (c and d) C/C–ZrC composite.

RMI could be operated at much lower temperature and the growth rate of ZrC would be greatly decreased. Consequently, the pores in the C/C preform could be sealed and dense matrix was formed after RMI.

3.2. Microstructure and composition

Fig. 1 shows the typical SEM micrographs of the C/C preform before RMI and the as-received C/C–ZrC composite. As can be seen, there are two kinds of pores in the C/C preform. The big pores exist among the carbon fiber bundles and the small pores exist inside the carbon fiber bundles (Fig. 1(a) and (b)). After alloyed melt infiltration, both types of pores were filled. Two kinds of microstructure were formed resulted from the reaction between the PyC and Zr–Si alloy. One seems rough and distributes around the PyC inside the pores in the C/C preform and the other seems comparatively flat and locates in the middle of pores surrounded by the rough one. EDS analysis was carried out to confirm the composition. The results are shown in Fig. 2. It is indicated that the rough one was composed of zirconium and carbon and the atom composition was 34:66. It was the phase ZrC derived from the reaction between PyC and zirconium. The flat one was composed of silicon and zirconium, with an atom proportion of 32:68. It might be the phase Zr_2Si. No region composed of pure zirconium was found.

XRD phase analysis of the C/C–ZrC composite is shown in Fig. 3. It is indicated that the phases in the composite are carbon, ZrC and Zr_2Si, respectively. No detectable zirconium peak was seen in the XRD patterns. The broad carbon peak refers to the carbon fibres and unreacted PyC. The main phase ZrC is resulted from the reaction between zirconium and PyC. The phase Zr_2Si derived from the reaction between residual silicon and zirconium. The phase determination by XRD confirmed the results from EDS analysis.

ZrC and Zr_2Si phases were formed resulted from the reaction between the PyC and Zr–Si alloy after RMI process. ZrC distributes around PyC inside the pores in the C/C preform

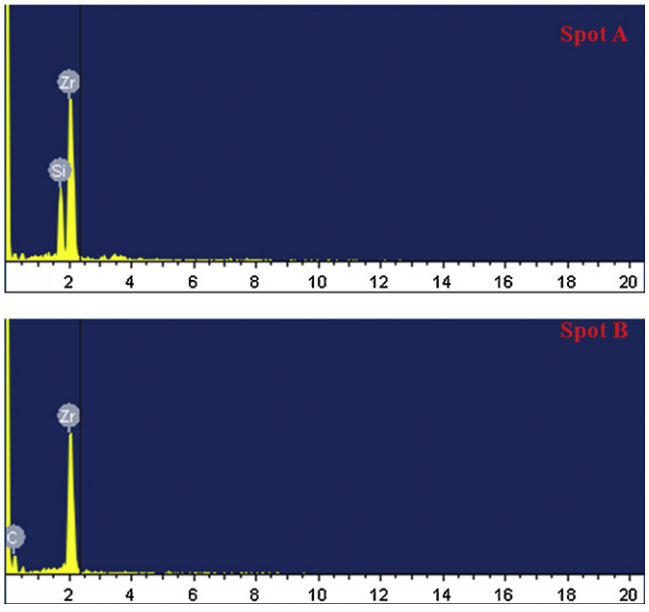

Fig. 2. EDS analysis of the obtained C/C–ZrC composite: (a) spot A and (b) spot B in Fig. 1(b).

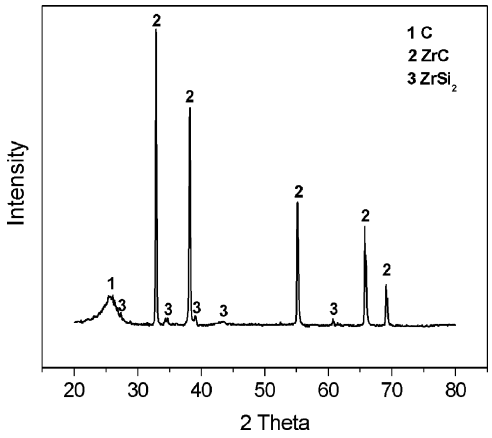

Fig. 3. XRD patterns of the as-received C/C–ZrC composite.

and Zr_2Si locates in the middle of pores surrounded by ZrC (Fig. 1). It is believed that the formation and distribution of the phases are concerned with the reaction ability among silicon, zirconium and carbon. The reactions with the thermodynamic calculations are as follows:

$$C(s) + Zr(s) \rightarrow ZrC(s), \quad \Delta G_{1800\,^{\circ}C} = -180.1\,kJ/mol \quad (1)$$

$$C(s) + Si(l) \rightarrow SiC(s), \quad \Delta G_{1800\,^{\circ}C} = -55.9\,kJ/mol \quad (2)$$

$$Si(l) + 2Zr(s) \rightarrow Zr_2Si(s), \quad \Delta G_{1800\,^{\circ}C} = -243.9\,kJ/mol \quad (3)$$

Known from the thermodynamic calculations, the formation of ZrC according to Eq. (1) and Zr_2Si according to Eq. (3) are much more favorable than that of SiC according to Eq. (2) because of the more negative Gibbs free energy. The formation and distribution of the phases in the C/C–ZrC composite during the RMI process could be explained in Fig. 4. When the sample is heated to the RMI temperature (1800 °C), the eutectic Zr–Si alloyed melt homogenously infiltrates into the porous C/C preform (Fig. 4(b)). Zirconium in the melt prefers to react with PyC at the beginning and a ZrC layer is formed around the PyC. The melt and PyC are separated by the reaction-formed ZrC layer (Fig. 4(c)). Carbon atoms diffuse through the ZrC

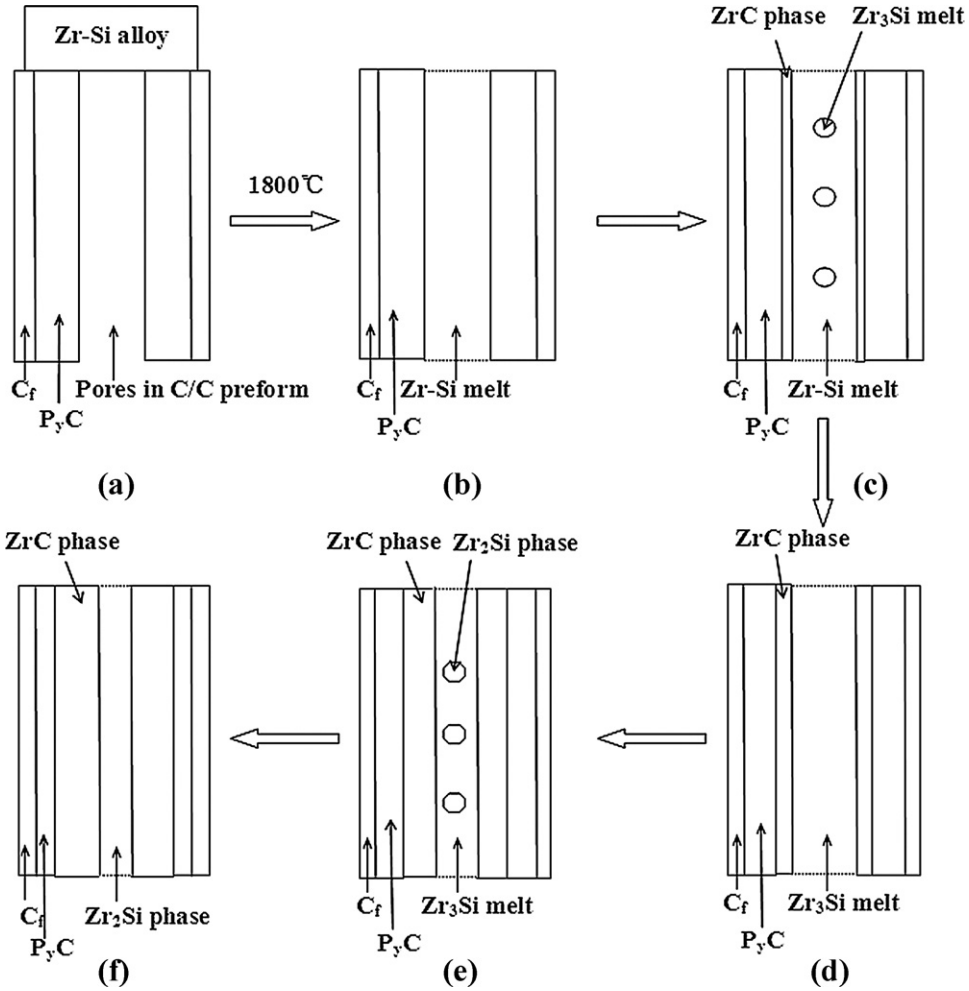

Fig. 4. Schematic of the microstructure formation mechanism of the C/C–ZrC composite during the RMI process (1800 °C, 30 min): (a) C/C preform and Zr–Si alloy before RMI starts, (b) infiltration of the eutectic Zr–Si melt into C/C preform at 1800 °C, (c) ZrC layer is formed around the PyC by the reaction between zirconium and PyC. The eutectic Zr–Si melt begins to change to Zr_3Si melt due to the decrease of the zirconium concentration, (d) growth of the ZrC layer and the total formation of Zr_3Si melt, (e) growth of ZrC layer and the formation of Zr_2Si in the Zr_3Si melt due to the further decrease of the zirconium concentration, and (f) total transformation of Zr_3Si melt into Zr_2Si phase and final microstructure at room temperature with ZrC distributing around the PyC inside the pores of C/C preform and Zr_2Si locating in the middle parts of the pores surrounded by ZrC.

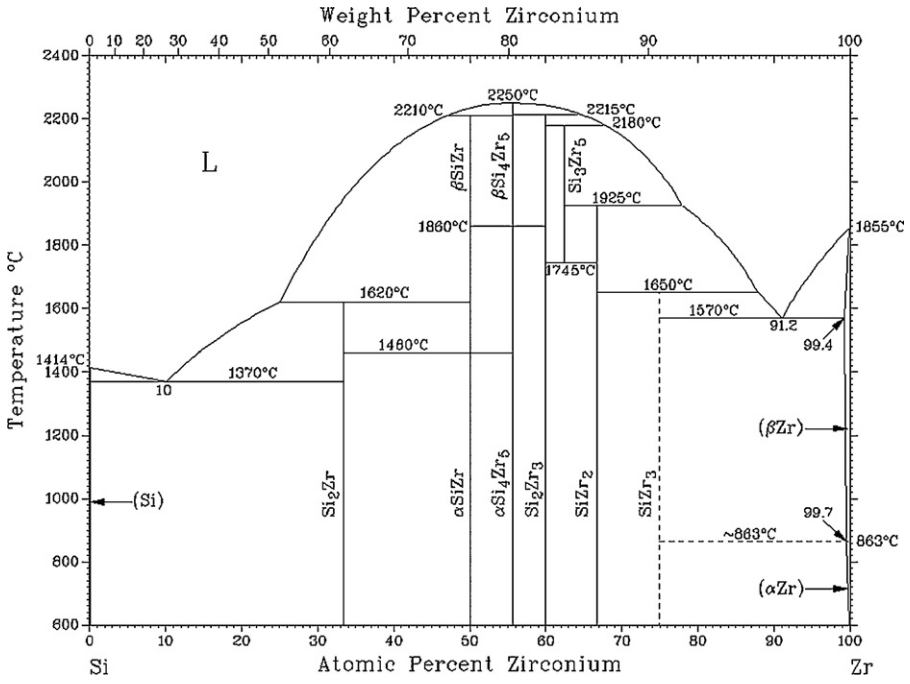

Fig. 5. Phase diagram of Zr–Si system.

layer and arrive at the interface between ZrC and the melt, and the subsequent reaction continues. With the proceeding of the reaction between zirconium and carbon, the concentration of zirconium in the melt decreases and Zr_3Si phase derived from the reaction of silicon with zirconium begins to precipitate form the melt (Fig. 4(c)), which is indicated by the phase diagram of Zr–Si system (Fig. 5). Zr_3Si phase, with the melting point of 1650 °C, is in the liquid condition at the RMI temperature. Atoms in the melt diffuse rapidly and the reaction between zirconium and carbon still progresses at a rather high speed. With the further decrease of the zirconium content in the melt, all the eutectic Zr–Si melt changes to Zr_3Si melt and then the Zr_3Si melt totally transfers to Zr_2Si phase due to the significant decrease of zirconium content (Fig. 4(d) and (e)). Zr_2Si, with the melting point of 1925 °C, is in solid state during the RMI process. Atoms in the solid Zr_2Si diffuse slowly and the formation of ZrC goes along at a rather low speed. Consequently, ZrC and Zr_2Si were formed in the as-received C/C–ZrC composite after RMI process (1800 °C, 30 min). ZrC distributes around the PyC and Zr_2Si locates in the middle of pores surrounded by ZrC (Fig. 4(f)).

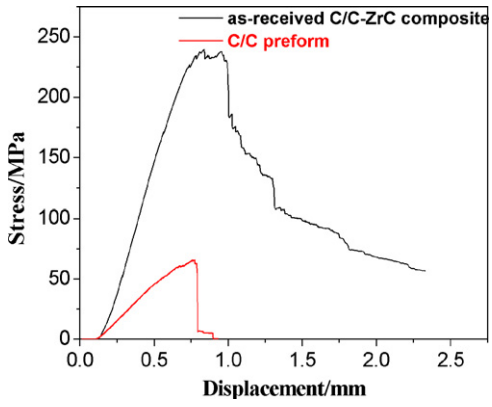

Fig. 6. Typical stress–deflection curves of the C/C preform and the C/C–ZrC composite.

3.3. Mechanical properties

Typical stress–deflection curves derived from the bending test for the C/C preform and C/C–ZrC composite are shown in Fig. 6. The flexural strength of C/C–ZrC composites is 239.5 MPa. For the curve of C/C–ZrC composite, an initial quasi-linear elastic region is followed by an increasing nonlinear stress up to a maximum. After reaching the maximum value, the stress decreases gradually. It shows a pseudo-ductile fracture behavior. Compared with the C/C–ZrC composite, the C/C preform just shows a quasi-linear elastic region, followed by a sharp decrease of the stress after it reaching the maximum value.

SEM photographs of the fracture surfaces of the C/C preform and the C/C–ZrC composite after the bending test are shown in Fig. 7. As can been seen, PyC presents very strong adherence to the carbon fibres in the C/C preform (Fig. 7(b)). Crack propagation within the matrix cannot be stopped or deflected around carbon fibres, thus the C/C preform presents a flat fracture surface (Fig. 7(b)). However, a great amount of carbon fibres are pulled out in the C/C–ZrC composite (Fig. 7(c)). The residual PyC presents lower adherence to carbon fibres after RMI and the reaction-formed ZrC does not adhere to the residual PyC tightly enough because of the large mismatch of coefficient of thermal expansion (CTE) between PyC and ZrC (CTE_C = 1.2 ppm/K, CTE_{ZrC} = 6.9 ppm/K). Therefore, the carbon fibres tend to split from the matrix and the crack formed in the matrix deflects along the interfaces with lower adherence. Consequently, the C/C–ZrC composite is toughed and shows a pseudo-ductile fracture behavior.

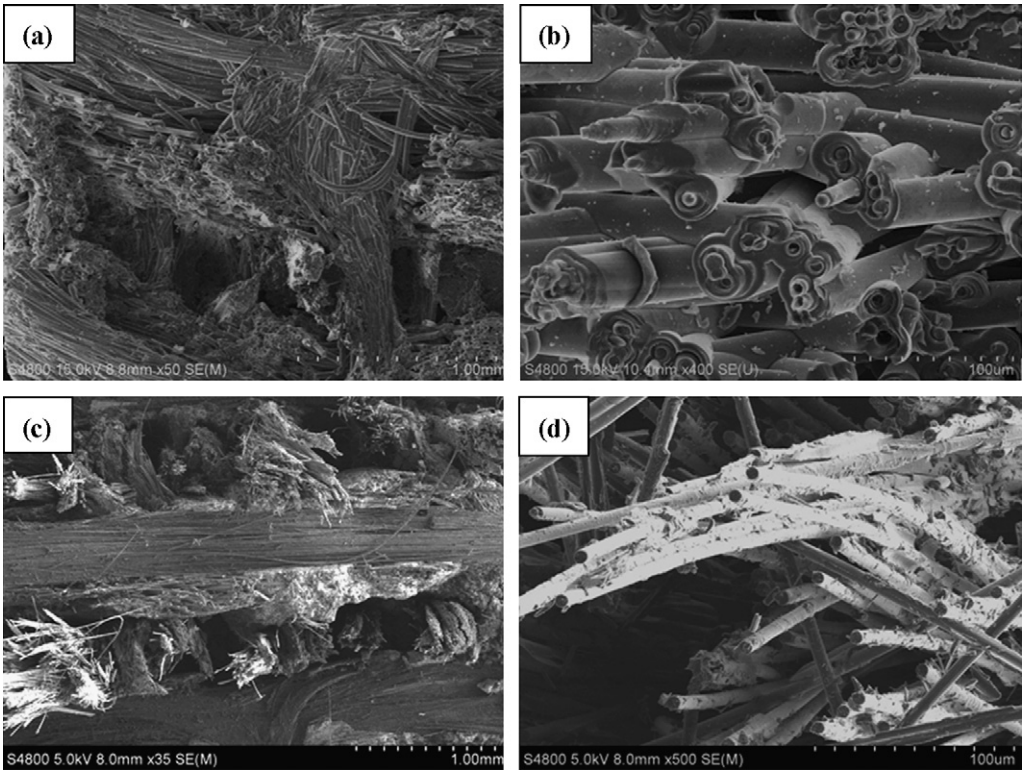

Fig. 7. SEM photographs of the fracture surfaces: (a and b) C/C preform and (c and d) C/C–ZrC composite.

3.4. Ablation resistance properties

A pulsed laser was used to test the ablation properties of the as-received C/C–ZrC composite. The ablation was sustained for 20 s. The linear ablation rate of the C/C–ZrC composite is listed in Table 2, which was calculated by the eroded depth at the ablation center dividing the ablation time. As comparison, the linear ablation rates of C/SiC, C/SiC–ZrB_2, C/SiC–TaC and C/SiC–ZrB_2–TaC composites are also listed in Table 1. XRD phase analysis of the C/C–ZrC composite after ablation is shown in Fig. 8. SiO_2 and ZrO_2 (including m-ZrO_2 and c-ZrO_2) were formed after the laser testing. The phase SiO_2 derived from the oxidation of Zr_2Si, and the phase ZrO_2 was formed due to the oxidation of ZrC and Zr_2Si in the C/C–ZrC composite. The possible reactions during the ablation testing are as follows [19,20]:

$$ZrC(s) + (3/2)O_2(g) = ZrO_2(s) + CO(g) \quad (R1)$$

$$ZrO_2(s) = ZrO_2(l) \quad (R2)$$

$$ZrO_2(l) = ZrO_2(g) \quad (R3)$$

$$C(s) + (1/2)O_2(g) = CO(g) \quad (R4)$$

$$CO(g) + (1/2)O_2(g) = CO_2(g) \quad (R5)$$

$$Zr_2Si(s) + 3O_2(s) = 2ZrO_2(s) + SiO_2(s) \quad (R6)$$

$$SiO_2(s) = SiO_2(l) \quad (R7)$$

$$SiO_2(l) = SiO_2(g) \quad (R8)$$

Table 2
Linear ablation rates of C/ZrB_2–SiC, C/SiC–TaC, C/SiC, C/SiC–ZrB_2–TaC and C/C–ZrC composites.

Materials	Linear ablation rate (mm/s)
C/ZrB_2–SiC [16]	0.066
C/SiC–TaC [17]	0.038
C/SiC [17]	0.083
C/SiC–ZrB_2–TaC [18]	0.026
C/C–ZrC	0.028

Fig. 9 shows the surface morphologies of the ablated C/C–ZrC composite. As can be seen, a white layer was formed in the central region of the ablated surface. EDS analysis indicated that it was composed of zirconium and oxygen. It is believed that this layer is ZrO_2 resulted from the reactions (R1) and (R6). No detectable silicon was found. With the laser power of 1000 W/mm^2, the center region was instantly heated to a very high temperature, approximately 3000 °C. SiO_2 resulted from reaction (R6) immediately gasified (boiling point of SiO_2 is 2230 °C [21]) and no detectable SiO_2 was found. At the brim region, the temperature was lower than the central region and spherical SiO_2 was found on the carbon fibres because of the bad wetting property between carbon and SiO_2. Near to the ablation center, the temperature is low and the C/C–ZrC composite was just slightly oxidized. The ZrO_2 and SiO_2 resulted from reactions (R1) and (R6) in the ablation region help to improve the ablation resistance properties of the C/C–ZrC composite. For the one hand, the evaporation of SiO_2 and a

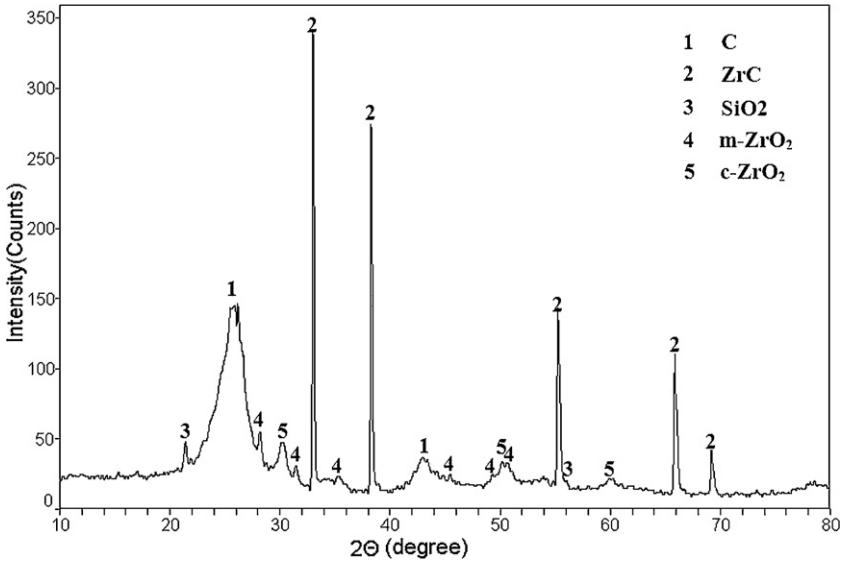

Fig. 8. XRD analysis of the as-received C/C–ZrC composite after ablation.

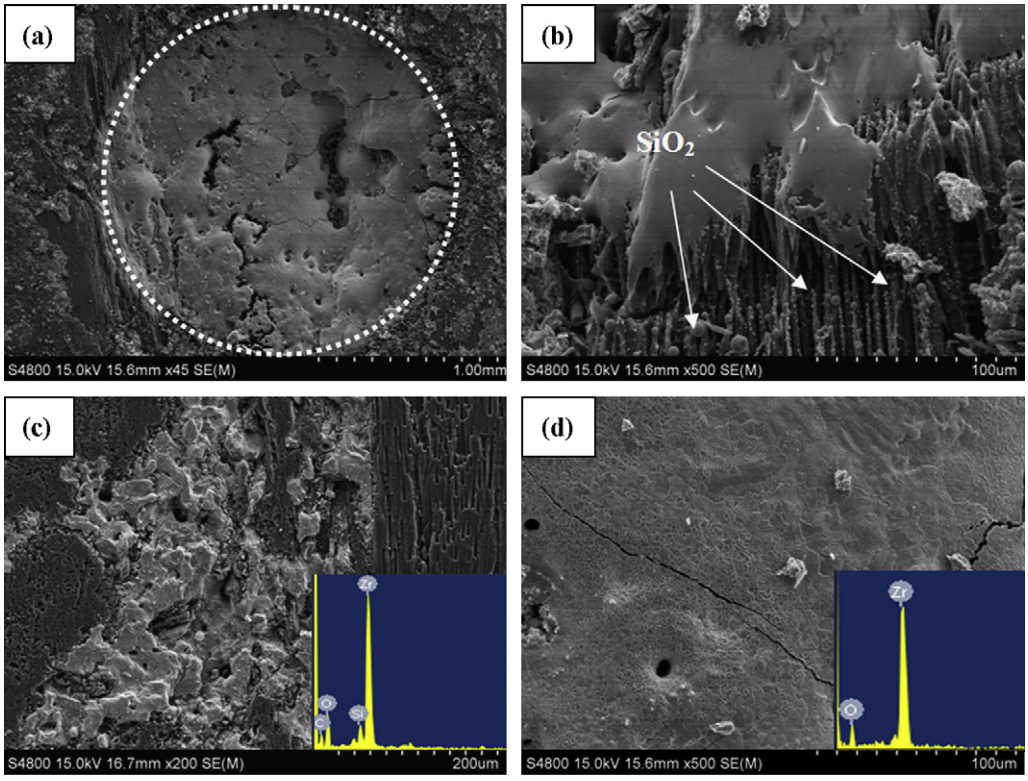

Fig. 9. Morphologies of the as-received C/C–ZrC composite after ablation: (a) 45×, (b) the brim region, (c) the region near to the ablation center, and (d) the central region, with EDS pattern of the surface.

spot of ZrO_2 entrained partial quantity of heat on the surface of the sample. For the other, the ZrO_2 is in liquid state at the ablated temperature and could flow onto the carbon fibres and seal the cracks and holes in the C/C–ZrC composite. The diffusion of the oxygen to the inner of the C/C–ZrC composite would be blocked by the liquid ZrO_2 barrier layer. Therefore, the C/C–ZrC composite are protected and present excellent ablation resistant performance.

4. Conclusion

C/C–ZrC composite was prepared by chemical vapor infiltration combined with alloyed reactive melt infiltration. Carbon fibre preform was infiltrated by the zirconium–silicon melt. The phases in the C/C–ZrC composite are carbon, ZrC and Zr_2Si, respectively. The investigation by thermodynamics and phase diagram indicates that ZrC distributes around the

PyC inside the pores in C/C preform and Zr_2Si locates in the middle of pores surrounded by ZrC. The density of the C/C–ZrC composite is 2.46 g/cm^3 and the open porosity is 5%. The flexural strength of the C/C–ZrC composite is 239.5 MPa. A great amount of fibres were pulled out on the fracture surface and the composite presented a pseudo-ductile fracture behavior. The ablation property of C/C–ZrC composite was tested by a pulse laser. The linear ablation rate is 0.028 mm/s. A ZrO_2 barrier layer was formed on the ablation surface and the C/C–ZrC composite presented excellent ablation resistance.

References

[1] J.R. Strife, J.E. Sbeehan, Ceramic coatings for carbon–carbon composites, American Ceramic Society Bulletin 67 (2) (1988) 369–374.

[2] J.E. Sheehan, Oxidation protection for carbon fibre composites, Carbon 27 (5) (1989) 709–715.

[3] L.G. Adam, G.F. William, E.H. Gregory, High-strength zirconium diboride-based ceramics, Journal of the American Ceramic Society 87 (2004) 1170–1172.

[4] R.L. Stanley, J.O. Elizabeth, C.H. Michael, D.K. James, S. Mrityunjay, A.S. Jonathan, Evaluation of ultra-high temperature ceramics for aero-propulsion use, Journal of the European Ceramic Society 22 (2002) 2757–2767.

[5] S.F. Tang, J.Y. Deng, S.J. Wang, W.C. Liu, K. Yang, Ablation behaviors of ultra-high temperature ceramic composites, Materials Science and Engineering A 465 (2007) 1–7.

[6] M. Esfehaniana, J. Günstera, F. Moztarzadehb, J.G. Heinrich, Development of a high temperature Cf/XSi_2–SiC (X = Mo, Ti) composite via reactive melt infiltration, Journal of the European Ceramic Society 27 (2007) 1229–1235.

[7] E. Fitzer, R. Gadow, Fibre-reinforced silicon carbide, American Ceramic Society Bulletin 65 (1986) 326–335.

[8] A. Sayir, Carbon fibre reinforced hafnium carbide composite, Journal of Materials Science 39 (2004) 5995–6003.

[9] Z.K. Chen, X. Xiong, G.D. Li, Y.L. Wang, Ablation behaviors of carbon/carbon composites with C–SiC–TaC multi-interlayers, Applied Surface Science 255 (2009) 9217–9223.

[10] E.O. Einset, Analysis of reactive melt infiltration in the processing of ceramics and ceramic composites, Chemical Engineering Science 53 (5) (1998) 1027–1039.

[11] W. Krenkel, Cost effective processing of composites by melt infiltration (LSI process), Ceramic Engineering and Science Proceedings 22 (2001) 443–454.

[12] L.H. Zou, N. Wali, J.M. Yang, N.P. Bansal, Microstructural development of a C_f/ZrC composite manufactured by reactive melt infiltration, Journal of the European Ceramic Society 30 (2010) 1527–1535.

[13] Y. Wang, X.J. Zhu, L.T. Zhang, L.F. Cheng, Reaction kinetics and ablation properties of C/C–ZrC composites fabricated by reactive melt infiltration, Ceramics International 37 (4) (2011) 1277–1283.

[14] L.M. Adelsberg, L.H. Cadoff, J.M. Tobin, Kinetics of the zirconium–carbon reaction at temperatures above 2000 °C, Metallurgical and Materials Transactions 236 (1966) 973–977.

[15] J.P. Wang, Z.H. Jin, J.M. Qian, G.J. Qiao, Research progress on mechanism and kinetics of C/C–SiC composites prepared by reactive melt infiltration, Journal of the Chinese Ceramic Society 33 (98) (2005) 1120–1126.

[16] Y.G. Wang, W. Liu, L.F. Cheng, L.T. Zhang, Preparation and properties of 2D C/ZrB_2–SiC ultra high temperature ceramic composites, Materials Science and Engineering A 524 (2009) 129–133.

[17] Y. Wang, Y.D. Xu, Y.G. Wang, L.F. Cheng, L.T. Zhang, Effects of TaC addition on the ablation resistance of C/SiC, Materials Letters 64 (2010) 2068–2071.

[18] L.L. Li, Y.G. Wang, L.F. Cheng, L.T. Zhang, Preparation and properties of 2D C/SiC–ZrB_2–TaC composites, Ceramics International 37 (2011) 891–896.

[19] X.T. Shen, K.Z. Li, H.J. Li, H.Y. Du, W.F. Cao, F.T. Lan, Microstructure and ablation properties of zirconium carbide doped carbon/carbon composites, Carbon 48 (2010) 344–351.

[20] H.F. Hu, Q.K. Wang, Z.H. Chen, C.R. Zhang, Y.D. Zhang, J. Wang, Preparation and characterization of C/SiC–ZrB_2 composites by precursor infiltration and pyrolysis process, Ceramics International 36 (2010) 1011–1016.

[21] D. Fang, Z.F. Chen, Y.D. Song, Z.G. Sun, Morphology and microstructure of 2.5 dimension C/SiC composites ablated by oxyacetylene torch, Ceramics International 35 (2009) 1249–1253.